catalysts

MDPI

Communication

Au Nanoparticles Supported on Mn- or/and La-Doped CeO_2 Nanorods for One-Step Oxidative Esterification of Methacrolein and Methanol to Methyl Methacrylate

Haojian Zhang [1,2]

[1] School of Materials and Chemical Engineering, Ningbo University of Technology, Ningbo 315211, China; zhj@nbut.edu.cn; Tel.: +86-574-8708-1240
[2] Zhejiang Institute of Tianjin University, Ningbo 315201, China

Abstract: Mn- or/and La-doped CeO_2 nanorods supporting Au catalysts were prepared using the hydrothermal method and deposition precipitation (DP) method and applied to the direct oxidative esterification of methacrolein (MAL) and methanol into methyl methacrylate (MMA). Various characterization techniques such as N_2-physical adsorption, X-ray diffraction (XRD), transmission electron microscopy (TEM), X-ray photoelectron spectroscopy (XPS), H_2 temperature programmed reduction (TPR) and CO_2 temperature programmed desorption (TPD) were utilized to analyze the structural properties, reducibility and basicity of Au catalysts. The catalyst with Mn doping only showed the best performance, and particularly the highest conversion, while the catalyst with Mn and La doping showed the highest selectivity.

Keywords: CeO_2 nanorods; dope; Mn; La; methyl methacrylate; oxidative esterification

Citation: Zhang, H. Au Nanoparticles Supported on Mn- or/and La-Doped CeO_2 Nanorods for One-Step Oxidative Esterification of Methacrolein and Methanol to Methyl Methacrylate. *Catalysts* **2023**, *13*, 767. https://doi.org/10.3390/catal13040767

Academic Editors: Zhongzhe Wei and Yutong Gong

Received: 9 March 2023
Revised: 12 April 2023
Accepted: 13 April 2023
Published: 18 April 2023

1. Introduction

Methyl methacrylate (MMA) is an important organic chemical intermediate, which is widely used for producing acrylic plastics (e.g., poly methyl methacrylate, PMMA), polymer dispersions for paints and coatings and other important fine chemicals. The industrial production of MMA is mainly through the acetone cyanhydrin method (ACH process), the ethylene carbonylation method and the isobutylene oxidation method [1,2]. However, the former two methods suffer from serious environmental and economic drawbacks, such as the use of highly toxic hydrogen cyanide and the harsh conditions of the transportation and storage of ethylene, which mean an environmentally benign route for the production of MMA is urgently needed [3]. The two-step oxidation process of the isobutylene oxidation method, including the oxidation of isobutylene to methacrolein (MAL) and the oxidative esterification of MAL with methanol in oxygen atmosphere, is one of the most attractive routes for the production of MMA.

Supported Pd-based catalysts have been widely considered because of their mild operating conditions. A wide variety of materials such as $CaCO_3$, ZnO, Al_2O_3, SiO_2-$A1_2O_3$-MgO, MgO-SBA-15, hydrophobic copolymer and other supports have been exploited for Pd-based catalysts [4–9]. Usually, additives such as Pb, Bi, Ag and alkaline earth metals are added to improve the catalytic performance. However, Pb is quite toxic, and an additional alkali is usually required. In most cases, the use of a large excess of methanol may cause high energy consumption in the following separation process. Therefore, the design of a new catalyst with excellent catalytic performance for the oxidative esterification of MAL is an important and urgent task.

Compared with the Pd-based catalysts, Au-based catalysts have attracted extensive attention due to their excellent catalytic properties in terms of selectivity for the oxidative esterification of MAL. Efforts are mainly focused on exploiting suitable supports such as SiO_2-Al_2O_3-MgO, MgO, hydroxyapatite, La_2O_3 and Ce-based oxides [10–20] with aims to

adjust the particle size of Au, the interaction between active components (Au nanoparticles) with the support, the reducibility, as well as the acidic–basic properties for obtaining a catalyst with excellent catalytic performance under base-free conditions. A $AuNiO_X$ catalyst with a core–shell structure supported on SiO_2-$A1_2O_3$-MgO showed high selectivity (around 98%) of MMA, while the conversion of MAL was only 62%, as reported by Suzuki et al. [10]. Wang et al. found supports with high densities of basic sites, particularly the stronger basic sites, exhibited good catalytic performances [12]. Thus, the Au/MgO catalyst possessed the MAL conversion of 98% and MMA selectivity of 99%. Au nanoparticles dispersed on needle-like hydroxyapatite and La_2O_3 nanorods exhibited higher catalytic activity and selectivity under mild reaction conditions with strong interaction, abundant in surface defects and acid–base sites [13,15].

CeO_2-based oxides have been widely applied as supports or catalysts for different kinds of reactions due to their high oxygen storage/release capacities. Doping transition metal atoms (such as Mn, Zr) into the CeO_2 crystal lattice is beneficial for forming oxygen vacancy clusters on CeO_2-based oxide surfaces and constructing more defect sites, so as to significantly promote the formation of reactive oxygen species and improve the catalytic performance [17–19]. Meanwhile, such a metal-doping strategy has many advantages in improving the potential reducibility, basicity and oxygen storage/release capabilities of supports [16–22]. Mn has been proved to be an excellent doping element for many reactions such as aldehyde oxidative esterification, CO oxidation and ammonia oxidation [18,22,23]. CeO_2-based solid solutions containing rare earth metals have been extensively studied for three-way catalyst (TWC) application and soot oxidation reaction [24–26]. Au nanoparticles supported on La-doped CeO_2-based oxides for the oxidative esterification of aldehydes have not been demonstrated.

Based on the above analysis, Mn- or/and La-doped CeO_2 nanorods supporting Au catalysts were prepared using the hydrothermal method and deposition precipitation (DP) method. The effects of different metal-doped supports on the performance were studied and correlated with the characterization results of catalysts.

2. Results and Discussion

2.1. Catalysts Characterization

The XRD patterns of the catalysts are shown in Figure 1. CeO_2 nanorods without doping and doping Mn or/and La are labeled as R-C, CM, CL and CML, respectively. Correspondingly, the supported Au catalysts are denoted as Au/R-C, Au/CM, Au/CL and Au/CML. Eight peaks at 28.5°, 33.1°, 47.5°, 56.3°, 59.1°, 69.4°, 76.7° and 79.1° are consistent with (111), (200), (220), (311), (222), (400), (331) and (420) of CeO_2 (ICDD, NO. 01-081-0792), respectively. Each catalyst has sharp diffraction peaks, indicating that the prepared support has high crystallinity. No diffraction peaks related to the doping Mn or/and La oxides are observed, indicating that the solid solution is formed due to the introduction of smaller M^+ (M = Mn or La) into the CeO_2 lattice. Except for Au/CM, no Au characteristic diffraction peak of plane (111) is found near 38.2°, indicating that Au nanoparticles are highly dispersed over the supports.

The physical and structural properties of the catalysts are illustrated in Table 1, including the BET surface area, pore volume, average pore size, Au content and Au NP size. As shown in Table 1, Au/R-C possesses the lowest surface area of 90 m^2/g. The surface area of Au/CM and Au/CL increases up to 103 m^2/g with Mn or La doping, consistent with the decrease in the crystallite size of support. The Au content of each catalyst is around 1.5%, lower than the experimental design value of 2%. This may be related to the washing process of using NH_4OH during the preparation of Au catalysts.

The morphology of the catalysts and particle size of Au were investigated by TEM images. As shown in Figure 2, doping with Mn or/and La does not affect the morphology of the support. All the catalysts are rod-like, and the metal particles Au are basically granular. The results of particle size statistics show that the average particle size of the Au/R-C

catalyst is 3.13 nm, that of the catalyst doped with Mn is 6.15 nm, that of the catalyst doped with La is 5.61 nm, and that of the catalyst doped with Mn and La is 5.96 nm.

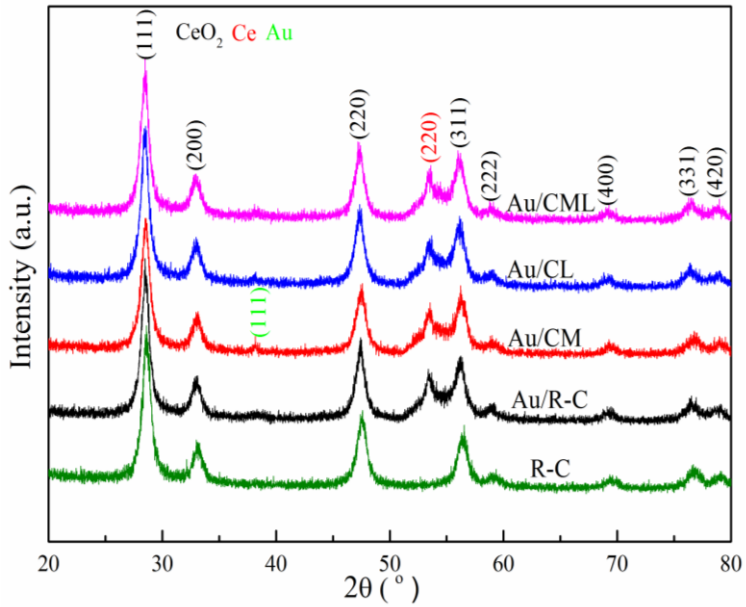

Figure 1. XRD patterns of the catalysts.

Table 1. Physical and structural properties of the catalysts.

Catalysts	Surface Area m^2/g	Pore Volume cm^3/g	Average Pore Size nm	Au Content [a] wt(%)	Crystallite Size of Support [b] nm
Au/R-C	90	0.50	23	1.44	24.2
Au/CM	103	0.49	19	1.47	21.9
Au/CL	103	0.45	17	1.49	21.4
Au/CML	96	0.39	15	1.44	23.8

[a] Analyzed by ICP-OES. [b] Calculated from the average of support planes of (111), (220) and (311) using Scherrer's equation.

As the size difference between Au particles and support is small in the TEM analysis, Au particles could be easily overlapped by support. Many Au particles are difficult to distinguish. It is not very suitable to determine the size distribution of Au by TEM alone. Therefore, the size of Au particles in the catalyst was characterized by STEM-EDS, and the uniform distribution of Au particles can be clearly seen as shown in Figure 3.

The XPS technology was used to study the valence state of Au and the relative surface atomic ratios of Ce. Figure 4 shows the XPS spectra of Au 4f, and Table 2 lists the binding energies of Au 4f for all catalysts. All of the samples have similar curves with two large peaks around at 83.5 and 87.2 eV, which belong to the binding energy peaks of Au $4f_{5/2}$ and Au $4f_{7/2}$ of metallic Au, respectively [27]. The metallic Au and the active oxygen species can enhance the oxidative esterification of aldehydes with methanol effectively [28,29].

Figure 5 represents the Ce 3d spectra of all catalysts. As the hybridization between O 2p levels and the partially occupied Ce 4f level [30], the photoelectron spectra of Ce 3d are very complex. The peaks of Ce 3d spectra are divided into two types of v and u, which correspond to Ce $3d_{5/2}$ and Ce $3d_{3/2}$, respectively [31,32]. Six peaks at the binding energies of 901.9 (u), 907.9 (u_2), 917.1 eV (u_3), 882.7 (v), 889.4 (v_2) and 898.7 eV (v_3) are assigned to the Ce^{4+} oxidation state, while other two peaks at the binding energies of 885.0 (v_1) and 903.5 eV (u_1) are assigned to the Ce^{3+} oxidation state [19]. The content of Ce^{3+} and Ce^{4+} can be calculated from the integrated peak area with respect to the total area of the spectra. Meanwhile, the ratio of Ce^{3+} to Ce^{4+} is obtained. All of these results are presented

in Table 2. The content of Ce^{3+} in Au/CM is 12.72%, while the content of Ce^{3+} in Au/R-C is the lowest, accounting for 7.97%. Usually, oxygen vacancies in Ce-based materials are generated by electron transfer between Ce^{3+} and Ce^{4+}. The higher the content of Ce^{3+}, the more oxygen vacancies exist in the material. From the above analysis, it can be concluded that the catalyst doped with Mn possesses the most oxygen vacancies, followed by the catalysts doped with Mn and La, and Au/R-C has the least oxygen vacancies.

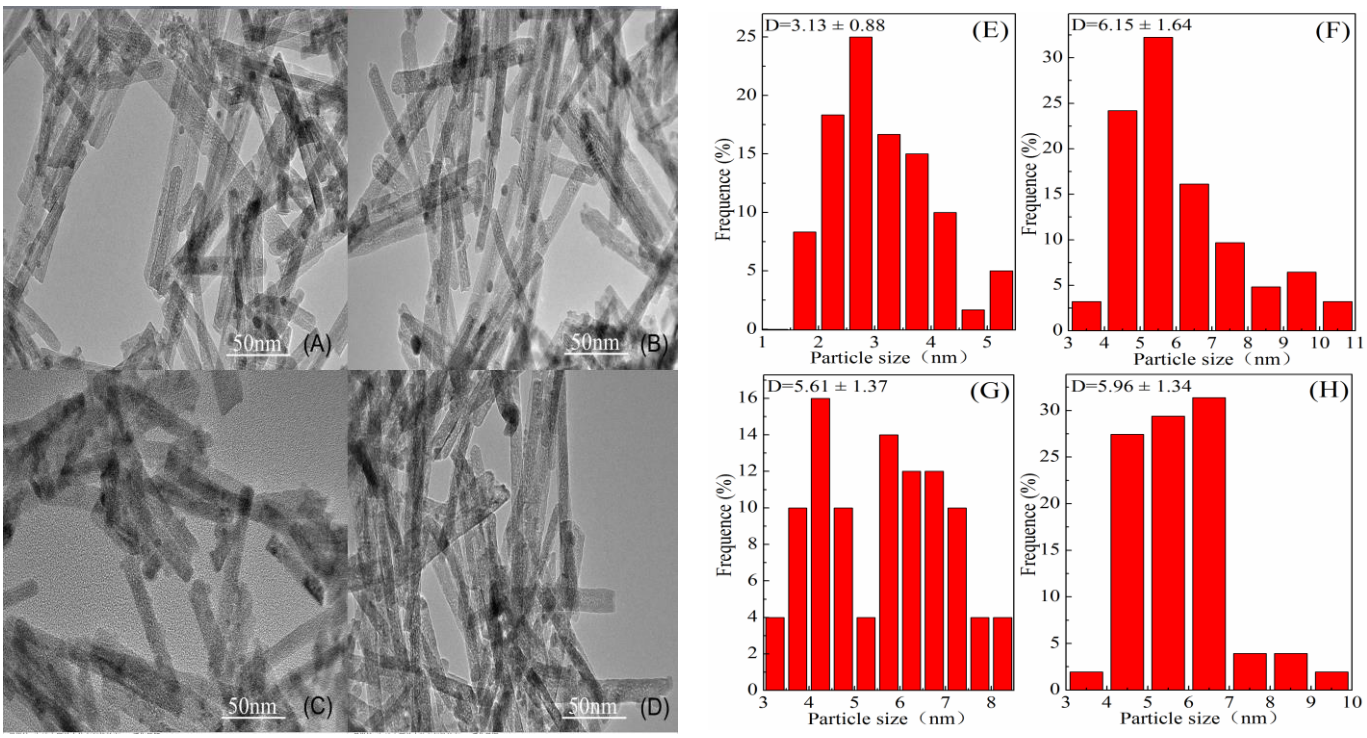

Figure 2. TEM micrographs and particle size distributions of the catalysts ((**A**,**E**) Au/R-C; (**B**,**F**) Au/CM; (**C**,**G**) Au/CL; (**D**,**H**) Au/CML).

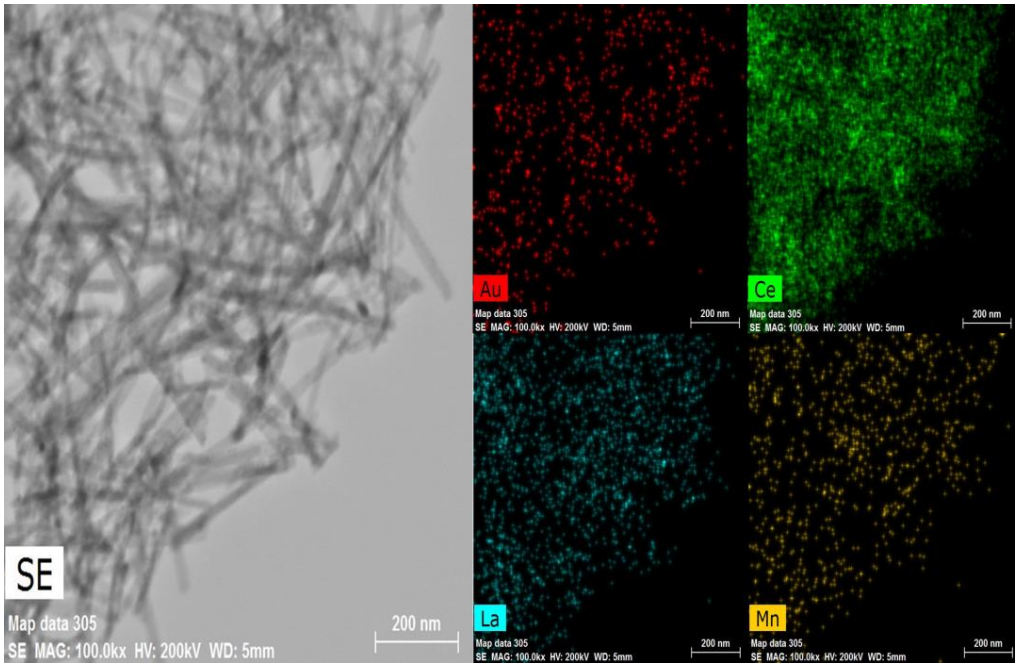

Figure 3. STEM-EDS maps of the Au/CML catalyst.

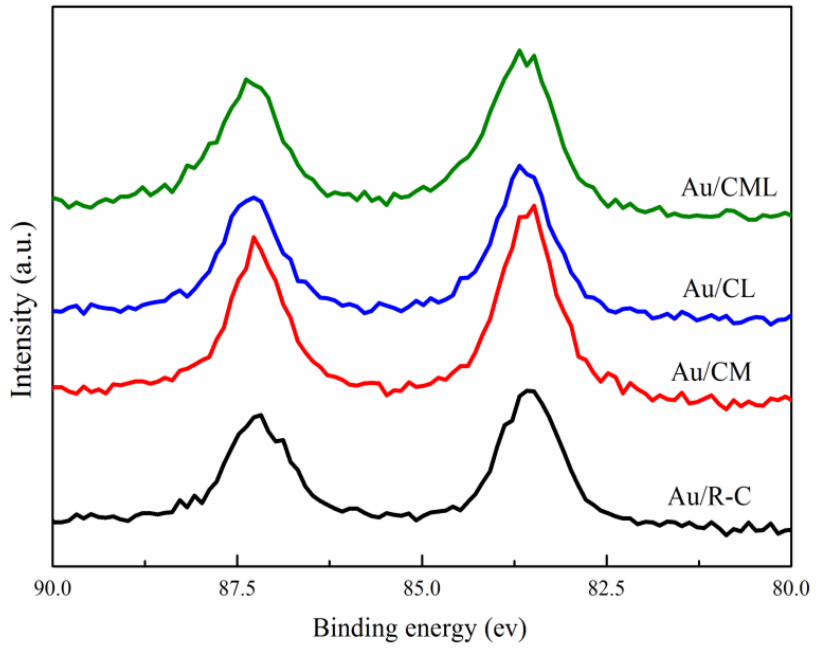

Figure 4. XPS spectra of Au 4f.

Table 2. Binding energies of Au and surface Ce species of the catalysts.

Catalysts		Au/R-C	Au/CM	Au/CL	Au/CML
Au species	Au $4f_{5/2}$ (ev)	87.20	87.23	87.29	87.33
	Au $4f_{7/2}$ (ev)	83.50	83.53	83.62	83.65
Ce species	Ce^{3+} (%)	7.97	12.72	9.04	12.4
	Ce^{4+} (%)	92.03	87.28	90.96	87.6
	R(Ce^{3+}:Ce^{4+}) (%)	8.66	14.57	9.94	14.16

The reducibility of the catalysts was investigated by H_2-TPR, as shown in Figure 6. There are mainly two well-separated peaks for all catalysts. The broad peak around 200 °C is assigned to the reduction in oxygen vacancies on the catalyst surface and the chemisorption's active oxygen species around Au particles. The peak after 650 °C corresponds to the bulk reduction in the oxide supports [33,34]. Au/CM and Au/CML present higher intensities of active oxygen species of the broad peak with the H_2 consumption of 1.021 and 0.851 mmol/g, respectively, than Au/CL and Au/R-C with H_2 consumption values of 0.791 and 0.704 mmol/g. Obviously, the amount of active oxygen species in the catalysts increases after doping with Mn or/and La, and Au/CM obtains the highest amount, which is consistent with the XPS results.

The surface basicity of supported Au catalysts was probed by CO_2-TPD. There are mainly three CO_2 desorption peaks in Figure 7. Peaks located at 130 °C, 300 °C and 570 °C are ascribed to weak, medium-strength and strong basic sites, respectively [13,16,35,36]. The amounts of basic sites were quantitatively calculated, and the data are summarized in Table 3. Clearly, the total basicity of the catalysts increases with Mn or/and La doping. Au/CML provides the highest amount of total basicity content. Basic sites mainly come from surface oxygen ions [15]. The introduction of Mn could enhance the number of oxygen ions on the surface [18]. Thus, Au/CML and Au/CM have higher total basicity levels, as the surface Mn content is 1.1% and 1.07%.

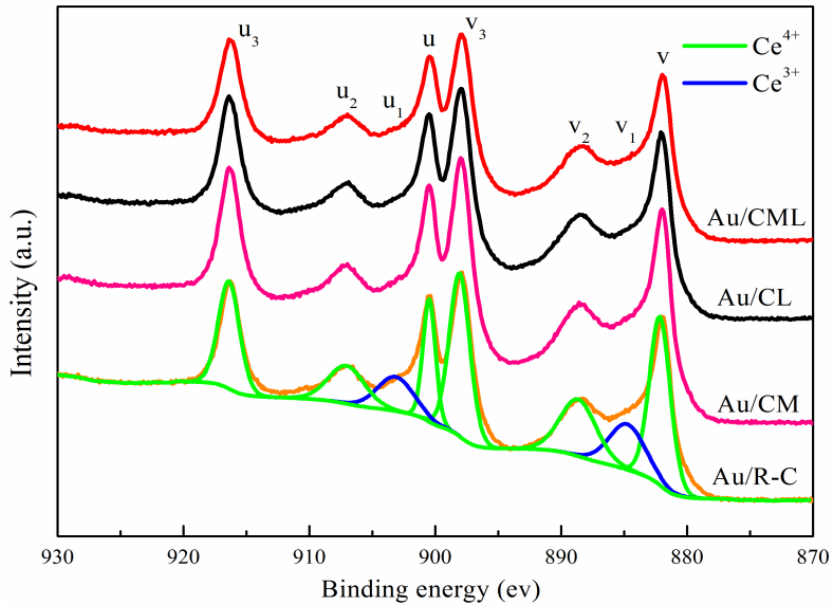

Figure 5. XPS spectra of Ce 3d.

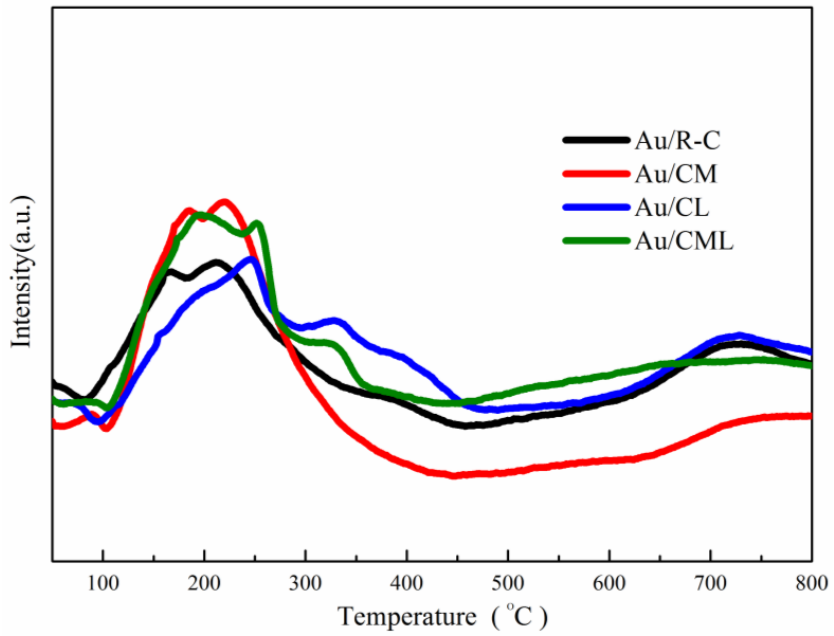

Figure 6. H_2-TPR profiles of catalysts.

Table 3. Surface basicity of the catalysts.

Catalysts	Total Basicity (mmol CO_2/g)
Au/R-C	0.692
Au/CM	0.817
Au/CL	0.737
Au/CML	0.989

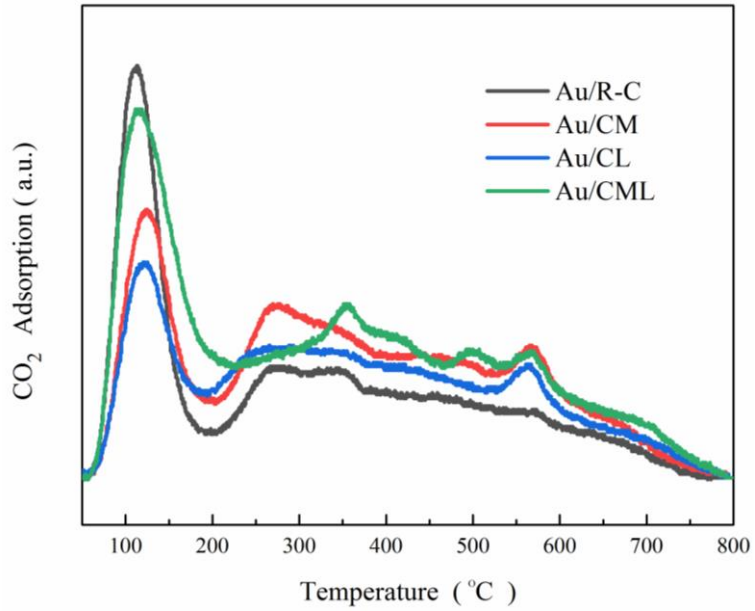

Figure 7. CO_2-TPD profiles of the prepared catalysts.

2.2. Catalytic Performance

The effects of doping with Mn or/and La on the activity of the catalysts are shown in Table 4. Mn and La have an apparent effect on the oxidative esterification of MAL to MMA. For the Au/R-C catalyst, the conversion of MAL is at a low level of 71.1%, and the selectivity of MMA is 91.6%. After only doping with Mn, the Au/CM catalyst exhibits the best performance with conversion of 98.6% and selectivity of 97.5%. Meanwhile, after only doping with La, the conversion and the selectivity reaches 91.5% and 98.0%, respectively. The conversion of the catalyst with Mn and La doping is 92.6%, which is slightly higher than that of the catalyst doped with La alone, and the selectivity increases to 98.9%.

Table 4. Catalytic performance of the catalysts [a].

Catalysts	MAL Conversion (%)	Selectivity [b] (%)		MMA Yield (%)
		MMA	Others	
Au/R-C	71.1	91.6	8.4	65.1
Au/CM	98.6	97.5	2.5	96.1
Au/CL	91.5	98.0	2.0	89.7
Au/CML	92.6	98.9	1.1	91.6

[a] Reaction conditions: catalyst 0.2 g, n (CH_3OH)/n (MAL) = 25:1, 80 °C, 0.30 MPa, 2 h. [b] Determined by GC analysis.

3. Materials and Methods

3.1. Synthesis of Mn- or/and La-Doped CeO_2 Nanorods and Supporting Au Catalysts

The Mn- or/and La-doped CeO_2 nanorods were prepared by the hydrothermal method. Taking the Mn- or La-doped CeO_2 nanorods' preparation as an example, a mixture containing 0.01 mol $Ce(NO_3)_3{\cdot}6H_2O$, 0.000526 mol $Mn(NO_3)_2{\cdot}4H_2O$ or 0.000526 mol $La(NO_3)_3{\cdot}6H_2O$ with an M/Ce (M = Mn or La) atomic ratio of 5:95 was introduced into a solution of NaOH (7.5 mol/L, 160 mL) and stirred vigorously for 0.5 h at room temperature. Then, the solution was transferred into a Teflon autoclave for hydrothermal reaction in an oven at 100 °C for 24 h. After centrifugation, washing and drying at 80 °C for 12 h, the obtained yellow powers were finally calcined at 400 °C for 4 h to obtain Mn- or La-doped CeO_2 nanorods. The Mn- and La-doped CeO_2 nanorods were prepared with the same method, except the Mn/La/Ce atomic ratio was 5:5:90.

The supporting Au catalysts were prepared using the deposition precipitation (DP) method. The $HAuCl_4$ (6.2 mL, 10^{-3} mol/L) was diluted with deionized water (160 mL). After adding 0.6 g of support, the pH of the solution was adjusted with Na_2CO_3 (0.1 mol/L) to 9. Then, the suspension was aged under continuous stirring at 70 °C for 4 h. Finally, the solid sample was filtered and washed with NH_4OH (4 mol/L) and deionized water to remove the remaining chlorine anion. The as-prepared catalyst was dried at 80 °C in a vacuum oven overnight and subsequently treated with 5%H_2-95%Ar at 150 °C for 5 h. The theoretical Au loading was 2%.

3.2. Catalysts Characterization

X-ray diffraction (XRD) measurements of the Au catalysts were made with a Rigaku D/max-2550 X-ray diffractometer (Tokyo, Japan) with a Cu Ka radiation source (λ = 0.154 nm) at 40 kV and 100 mA. The diffraction patterns were obtained between 20° and 80° at a scan rate of 4°/min.

A low-temperature N_2 physical adsorption/desorption experiment was performed by Micromerities ASAP 2020M (Norcross, GA, USA). Before the determination, all samples were treated at 150 °C and 1.33 Pa for about 6 h. The specific surface area was calculated using the Brunauer–Emmett–Teller (BET) equation, and the pore size distribution curve was calculated with the Barrett–Joyner–Halenda (BJH) method.

The hydrogen temperature programmed reduction (H_2-TPR) of the catalyst was tested using Micromeritics AutoChem II 2920 (Norcross, GA, USA). A 30 mg sample was loaded in a quartz reactor and treated with a 10% H_2-90% Ar (v/v) mixture from 50 °C to 800 °C (10 °C/min) under the flow of 50 mL/min.

The CO_2-TPD experiments were performed in the same system as used in H_2-TPR. In the CO_2-TPD experiment, the catalyst sample (50 mg) was firstly heated from room temperature to 200 °C (10 °C/min) for 60 min under an Ar flow rate of 50 mL/min and then cooled to 50 °C. After that, the sample was purged with CO_2 (10 mL/min) for 30 min. Finally, the sample was heated to 800 °C at a ramp of 10 °C/min for CO_2-TPD.

The X-ray photoelectron spectroscopy (XPS) test was completed on a Thermo NEXSA spectrometer (Waltham, MA, USA) using a monochromatic Al Kα source. The binding energies were calibrated using C1 speak at BE = 284.6 eV.

The elemental analysis of the Au catalysts was determined by using an Agilent ICP-OES 720 spectrometer (Santa Clara, CA, USA). The sample was dissolved in aqua regia before testing.

The catalyst samples were dispersed in ethanol using ultrasonic wave and deposited in the microscope grid. The TEM diagrams and elemental mapping measurements were analyzed by JEOLTEM 2100F (Tokyo, Japan).

3.3. Catalysts Evaluation

The oxidative esterification of MAL with methanol was performed in a continuous stirred tank reactor with a 50 mL polytetrafluoroethylene inner liner, into which the catalyst (0.2 g), MAL (10 mmol) and methanol (10 mL) were added. The reactor was purged with highly pure O_2 with a flow rate of 20 mL/min three times, which was maintained for 2 min each time. After that, the temperature of the reactor was increased to 80 °C. Then, O_2 was fed into the reactor under a stirring speed of 1000 rpm, and the relative pressure was kept at 0.3 MPa. After a 2 h reaction, the reactor was cooled rapidly in an ice water bath. Finally, the products were analyzed via a gas chromatograph of Shimadzu 2018 equipped with an AE-FFAP column (30 m × 0.32 mm × 0.5 μm) and an FID detector using ethanol as an internal standard for quantification.

4. Conclusions

Mn and La have significant influences on physico-chemical properties, reducibility and basicity behaviors, as well as the catalytic performances of CeO_2-based nanorods supported by Au catalysts. The characterization results indicate that the surface area,

oxygen vacancies, amount of active oxygen species and total basicity of the catalysts apparently increased with Mn or/and La doping. The amount of active oxygen species and total basicity are beneficial for improving the conversion and selectivity, respectively. The Au/CM catalyst with the highest amount of active oxygen species showed the best performance, and in particular, had the highest conversion of 98.6%. Au/CML had the highest selectivity of 98.9% as the highest total basicity of the catalyst.

Funding: This research was funded by State Key Laboratory of Molecular Engineering of Polymers (Fudan University), grant number K2022-12.

Data Availability Statement: Data are available in the article.

Acknowledgments: The author would like to thank the public testing platform of Ningbo University of Technology. Thanks for the technical support with the XRD, BET, ICP, TPD, TPR, TEM and XPS measurements.

Conflicts of Interest: The author declares no conflict of interest.

References

1. Nagai, K. New developments in the production of methyl methacrylate. *Appl. Catal. A Gen.* **2001**, *221*, 367–377. [CrossRef]
2. Yamamatsu, S.; Yamaguchi, T.; Yokota, K.; Nagano, O.; Chono, M.; Aoshima, A. Development of catalyst technology for producing methyl methacrylate (MMA) by direct methyl esterification. *Catal. Surv. Asia* **2010**, *14*, 124–131. [CrossRef]
3. Mahboub, M.J.D.; Dubois, J.L.; Cavani, F.; Rostamizadeh, M.; Patience, G.S. Catalysis for the synthesis of methacrylic acid and methyl methacrylate. *Chem. Soc. Rev.* **2018**, *47*, 7703–7738.
4. Yoshida, Y.; Mikami, Y.; Oh-Kita, M. Process for Producing Carboxylic Acid Esters and Catalyst. EP 0972759, 19 March 1998.
5. Diao, Y.Y.; Yan, R.Y.; Zhang, S.J.; Yang, P.; Li, Z.X.; Wang, L.; Dong, H.F. Effects of Pb and Mg doping in Al_2O_3-supported Pd catalyst on direct oxidative esterification of aldehydes with alcohols to esters. *J. Mol. Catal. A Chem.* **2009**, *303*, 35–42. [CrossRef]
6. Jiang, L.; Diao, Y.Y.; Han, J.X.; Yan, R.Y.; Zhang, X.P.; Zhang, S.J. MgO-SBA-15 supported Pd-Pb catalysts for oxidative esterification of methacrolein with methanol to methyl methacrylate. *Chin. J. Chem. Eng.* **2014**, *22*, 1098–1104. [CrossRef]
7. Wang, B.H.; Sun, W.J.; Zhu, J.; Ran, W.L.; Chen, S. Pd-Pb/SDB bimetallic catalysts for the direct oxidative esterification of methacrolein to methyl methacrylate. *Ind. Eng. Chem. Res.* **2012**, *51*, 15004–15010. [CrossRef]
8. Wang, B.H.; Li, H.; Zhu, J.; Sun, W.J.; Chen, S. Preparation and characterization of mono-/multi-metallic hydrophobic catalysts for the oxidative esterification of methacrolein to methyl methacrylate. *J. Mol. Catal. A Chem.* **2013**, *379*, 322–326. [CrossRef]
9. Wang, B.H.; Ran, W.L.; Sun, W.J.; Wang, K. Direct Oxidative Esterification of Aldehyde with Alcohol to Ester over Pd/Styrene-Divinyl Benzene Copolymer Catalyst. *Ind. Eng. Chem. Res.* **2012**, *51*, 3932–3938. [CrossRef]
10. Suzuki, K.; Yamaguchi, T.; Matsushita, K.; Iitsuka, C.; Miura, J.; Akaogi, T.; Ishida, H. Aerobic Oxidative Esterification of Aldehydes with Alcohols by Gold-Nickel Oxide Nanoparticle Catalysts with a Core-Shell Structure. *ACS Catal.* **2013**, *3*, 1845–1849. [CrossRef]
11. Costa, V.V.; Estrada, M.; Demidova, Y.; Prosvirin, I.; Kriventsov, V.; Cotta, R.F.; Fuentes, S.; Simakov, A.; Gusevskaya, E.V. Gold Nanoparticles Supported on Magnesium Oxide as Catalysts for the Aerobic Oxidation of Alcohols under Alkali-Free Conditions. *J. Catal.* **2012**, *292*, 148–156. [CrossRef]
12. Wan, X.; Deng, W.; Zhang, Q.; Wang, Y. Magnesia-Supported Gold Nanoparticles as Efficient Catalysts for Oxidative Esterification of Aldehydes or Alcohols with Methanol to Methyl Esters. *Catal. Today* **2014**, *233*, 147–154. [CrossRef]
13. Gao, J.; Fan, G.L.; Yang, L.; Cao, X.Z.; Zhang, P.; Li, F. Oxidative esterification of methacrolein to methyl methacrylate over gold nanoparticles on hydroxyapatite. *ChemCatChem* **2017**, *9*, 1230–1241. [CrossRef]
14. Li, J.; Li, H.Y.; Liu, Z.Y.; Akri, M.; Tan, Y.; Kang, L.L.; Chi, J.; Qiao, B.T.; Ding, Y.J. Synergic effect between gold and vanadate substituted hydroxyapatite support for synthesis of methyl methacrylate by one-step oxidative esterification. *Chem. Eng. J.* **2022**, *431*, 133207–133219. [CrossRef]
15. Paul, B.; Khatun, R.; Sharma, S.K.; Adak, S.; Singh, G.; Das, D.; Siddiqui, N.; Bhandari, S.; Joshi, V.; Sasaki, T.; et al. Fabrication of Au nanoparticles supported on one-dimensional (1D) La_2O_3 nanorods for selective Esterification of Methacrolein to Methyl Methacrylate with Molecular Oxygen. *ACS Sustinable Chem. Eng.* **2019**, *7*, 3982–3994. [CrossRef]
16. Li, Y.C.; Wang, L.; Yan, R.Y.; Han, J.X.; Zhang, S.J. Promoting effects of MgO, $(NH_4)_2SO_4$ or MoO_3 modification in oxidative esterification of methacrolein over Au/$Ce_{0.6}Zr_{0.4}O_2$-based catalysts. *Catal. Sci. Technol.* **2016**, *6*, 5453–5463. [CrossRef]
17. Tian, Y.; Li, Y.C.; Zuo, C.C.; Yin, D.F.; Wang, L.; Zheng, Y.X.; Huang, H.F.; Fu, Z.J.; Wang, M. Ionic-Liquid-Modified Porous Au/CeMnOx Nanorods for Methyl Methacrylate (MMA) Synthesis via Direct Oxidative Esterification. *ChemNanoMat* **2019**, *5*, 1361–1366. [CrossRef]
18. Tian, Y.; Li, Y.C.; Zheng, Y.X.; Wang, M.; Zuo, C.C.; Huang, H.F.; Yin, D.F.; Fu, Z.J.; Tan, J.; Zhou, Z.C. Nano-Au/MCeOx Catalysts for the Direct Oxidative Esterification of Methylacrolein to Methyl Esters. *Ind. Eng. Chem. Res.* **2019**, *58*, 19397–19405. [CrossRef]
19. Li, Y.C.; Tian, Y.X.; Ge, T.T.; Fu, Z.J.; Jiao, T.T.; Wang, M.; Huang, H.F.; Zuo, C.C. Direct oxidation esterification of methacrolein with methanol: Oxygen vacancy promotion of Zr-doped Au/CeO_2 nanorods. *Can. J. Chem. Eng.* **2020**, *3*, 767–774. [CrossRef]

20. Lim, S.; Kwon, S.; Kim, N.; Na, K. A Multifunctional Au/CeO_2-$Mg(OH)_2$ Catalyst for One-Pot Aerobic Oxidative Esterification of Aldehydes with Alcohols to Alkyl Esters. *Nanomaterials* **2021**, *11*, 1536. [CrossRef]
21. Lei, T.Q.; Guo, H.Y.; Miao, C.X.; Hua, W.M.; Yue, Y.H.; Gao, Z. Mn-doped CeO_2 Nanorod Supported Au Catalysts for Dehydrogenation of Ethane with CO_2. *Catalysts* **2019**, *9*, 119. [CrossRef]
22. Venkataswamy, P.; Jampaiah, D.; Mukherjee, D.; Aniz, C.U.; Reddy, B.M. Mn-doped ceria solid solutions for CO oxidation at lower temperatures. *Catal. Lett.* **2016**, *146*, 2105–2118. [CrossRef]
23. Qi, G.S.; Yang, R.T.; Chang, R. MnOx-CeO_2 mixed oxides prepared by co-precipitation for selective catalytic reduction of NO with NH_3 at low temperatures. *Appl. Catal. B* **2004**, *51*, 93–106. [CrossRef]
24. Gandhi, H.S.; Graham, G.W.; McCabe, E.W. Automotive exhaust catalysis. *J. Catal.* **2003**, *216*, 433–442. [CrossRef]
25. Kašpar, J.; Fornasiero, P.; Grazini, M. Use of CeO_2-based oxides in the three-way catalysis. *Catal. Today.* **1999**, *50*, 285–298. [CrossRef]
26. Bueno-López, A.; Krishna, K.; Makkee, M.; Moulijn, J.A. Enhanced soot oxidation by lattice oxygen via La^{3+}-doped CeO_2. *J. Catal.* **2005**, *230*, 237–248. [CrossRef]
27. Xiao, Z.R.; Ji, S.; Li, Y.T.; Hou, F.; Zhang, H.C.; Zhang, X.W.; Wang, L.; Li, G.Z. Tuning oxygen vacancies on mesoporous ceria nanorods by metal doping: Controllable magnetic property. *Appl. Surf. Sci.* **2018**, *455*, 1037–1044. [CrossRef]
28. Manzoli, M.; Menegazzo, F.; Signoretto, M.; Cruciani, G.; Pinna, F. Effects of synthetic parameters on the catalytic performance of Au/CeO_2 for furfural oxidative esterification. *J. Catal.* **2015**, *330*, 465–473. [CrossRef]
29. Xu, B.J.; Liu, X.Y.; Haubrich, J.; Friend, C.M. Vapour-phase gold-surface-mediated coupling of aldehydes with methanol. *Nat. Chem.* **2010**, *2*, 61–65. [CrossRef]
30. Katta, L.; Sudarsanam, P.; Mallesham, B.; Reddy, B.M. Preparation of silica supported ceria-lanthana solid solutions useful for synthesis of 4-methylpent-1-ene and dehydroacetic acid. *Catal. Sci. Technol.* **2012**, *2*, 995–1004. [CrossRef]
31. Burroughs, A.; Hamnett, A.; Orchard, A.F.; Thornton, G. Satellite structure in the X-ray photoelectron spectra of some binary and mixed oxides of lanthanum and cerium. *J. Chem. Soc. Dalton. Trans.* **1976**, *17*, 1686–1698. [CrossRef]
32. Guo, M.; Lu, J.Q.; Wu, Y.N.; Wang, Y.J.; Luo, M. UV and Visible Raman Studies of Oxygen Vacancies in Rare-Earth-Doped Ceria. *Langmuir* **2011**, *27*, 3872–3877. [CrossRef]
33. Fu, Q.; Saltsburg, H.; Flytzani-Stephanopoulos, M. Active Nonmetallic Au and Pt Species on Ceria-Based Water-Gas Shift Catalysts. *Science* **2003**, *301*, 935–938. [CrossRef]
34. Salvatore, S.; Simona, M.; Carmelo, C.; Cristina, S.; Alessandro, P. Catalytic combustion of volatile organic compounds on gold/cerium oxide catalysts. *Appl. Catal. B-Environ.* **2003**, *40*, 43–49.
35. Jia, L.S.; Gao, J.; Fang, W.P. Carbon dioxide hydrogenation to methanol over the pre-reduced $LaCr_{0.5}Cu_{0.5}O_3$ catalyst. *Catal. Commun.* **2009**, *10*, 2000–2003. [CrossRef]
36. Azzouz, A.; Nistor, D.; Miron, D.; Ursu, A.V.; Sajin, T.; Monette, F.; Niquette, P.; Hausler, R. Assessment of acid–base strength distribution of ion-exchanged montmorillonites through NH_3 and CO_2-TPD measurements. *Thermochim. Acta* **2006**, *449*, 27–34. [CrossRef]